

Full Paper

Design and Simulation of a Novel Magnetic Microactuator for Microrobots in Lab-On-a-Chip Applications

K. N. M. Perera^{*,a}, H. A. G. C. Premachandra^b, S. K. Dodampegama^a, and Y. W. R. Amarasinghe^{a,b}

^a Centre for Advanced Mechatronic Systems, University of Moratuwa, Katubedda 10400, Sri Lanka

^b Department of Mechanical Engineering, University of Moratuwa, Katubedda 10400, Sri Lanka

Email correspondence: nisalmper@gmail.com (K. N. M. Perera)

Received: 21 February 2022; Revised: 19 May 2022; Accepted: 20 May 2022; Published: 31 May 2022

Abstract

This article presents the design of a magnetic microactuator comprising soft magnetic material blocks and flexible beams. The modular layout of the proposed microactuator promotes scalability towards different microrobotic applications using low magnetic fields. The presented microactuator consists of three soft magnetic material (Ni-Fe 4750) blocks connected together via two Polydimethylsiloxane (PDMS) semi-circular beams. A detailed design approach is highlighted giving considerations toward compactness, range of motion and force characteristics of the actuator. The actuator displacement and force characteristics are approximately linear in the magnetic field strength range of 80-160 kA/m. It can achieve maximum displacements of 111.6 μm (at 160 kA/m) during extension and 10.7 μm (at 80 kA/m) during contraction under no-load condition. The maximum force output of the microactuator, computed through a contact simulation, was 404.3 nN at a magnetic field strength of 160 kA/m. The microactuator achieved stroke angles up to 18.4° in a study where the microactuator was integrated with a swimming microrobot executing rowing motion using an artificial appendage, providing insight into the capabilities of actuating untethered microrobots.

Keywords: Microactuator, magnetic, microrobotics, lab-on-a-chip

Introduction

The use of microrobots for in vitro applications is becoming wider due to their capabilities of object transportation, manipulation and sensing. When we consider in vitro applications, lab-on-a-chip (LOC) is a type of device which integrates one or more laboratory functions into a single chip. In these types of on-chip applications, microrobots can be incorporated to handle small objects with high accuracy and repeatability [1]. These microrobots are either tethered [2] or untethered [3, 4] depending on the actuation principle. It is beneficial if the microrobots can be actuated in an untethered manner, especially in LOC applications to achieve better mobility in the microfluidic environment [1, 5]. There are several actuation principles used in such untethered microrobots: photonic [6], magnetic [7, 8], electrostatic [9], acoustic [10], and combinations of actuation principles [11, 12]. Among these principles, using magnetic fields for actuation provides means for various actuation methods [13].

Since magnetic fields can travel through water undisturbed, it is a suitable option of microfluidic on-chip applications. In addition, magnetic actuators are capable of producing larger forces along with larger strokes compared to other methods [14]. Due to these reasons, researchers have shown an interest in developing magnetically actuated microactuators. These research dates back to the 1990s with the fabrication of micromotors on silicon wafer [15, 16]. Chang et al. [14] and Judy et al. [17] were able to obtain

out-of-plane motions using electroplated permalloys at the initial stages of this research area, thus laying a solid foundation for further developments. The use of magnetic microactuators has evolved drastically since then due to their favorable characteristics in micron-scale. Liu et al. [18] has developed Polydimethylsiloxane artificial cilium doped with iron particles. They emphasize that the aforementioned cilia can be used for propulsion of microrobots and as a mixer in LOC applications. Recently, magnetically actuated microactuator networks consisting of Janus microparticles and soft links have been proposed highlighting the versatile design possibilities [19]. In another research, Feng et al. [20] have proposed a microactuator which utilizes microcoils and microsprings that can be used in portable electronic equipment and microsattellites.

Cugat et al. [21] highlight that scale reduction enables magnetic microactuators to perform well. According to them, the interaction between permanent magnets (or an external magnetic field) and soft magnetic materials is significantly improved due to scale reduction. Soft magnetic materials have very high permeability with low coercivity. Magnetization of these materials depends on the externally applied magnetic field. Permalloy is such a soft magnetic material which is a Nickel (Ni) and Iron (Fe) alloy. Permalloy shows excellent soft magnetic properties with near-zero magnetostriction, thus widely used in Micro Electro Mechanical Systems (MEMS) [22]. In the context of MEMS, soft magnetic materials are preferred over permanent magnets due to availability and manufacturability. Moreover, since soft magnetic materials do not require an initial magnetization, they are more stable for a longer period of time [23].

There are interesting applications of soft magnetic properties utilized in recent developments. The underlying actuation principle of most of the microrobots has been soft magnetism in both microfluidic and dry environments [8, 23-25]. Especially, a linear microactuator that can provide an untethered actuation scheme for swimming microrobots is an interesting route. In this research, we propose a design of a soft magnetic microactuator that can be used for actuating microrobots. It is a linear microactuator with soft magnetic blocks affixed to each other with semi-circular beams in a novel arrangement, paving the way for a compact design. The proposed microactuator was designed to operate in low magnetic fields (1-199 mT) in order to get the benefits of operating within this range such as low-cost implementation, simpler setups and increased adaptability [26]. This setup undergoes a linear motion when subjected to a spatially uniform external magnetic field. Depending on the direction of the external magnetic field, the soft magnetic blocks get magnetized as shown in Figure 1(a). The magnetic interaction forces between the soft magnetic blocks cause the setup to extend or contract. In the absence of an external magnetic field, the microactuator returns to its idle position Figure 1(b). The stroke length of the microactuator can be controlled by varying the external magnetic field strength. Here, we present the design methodology of the microactuator, giving emphasis to key aspects such as compactness, range of motion and force characteristics. After optimizing the actuator design parameters, the actuator displacement and force characteristics as well as the performance when integrated into a swimming microrobot are discussed. Furthermore, a fabrication methodology for the proposed actuator is presented. Finally, the conclusions about the work are given.

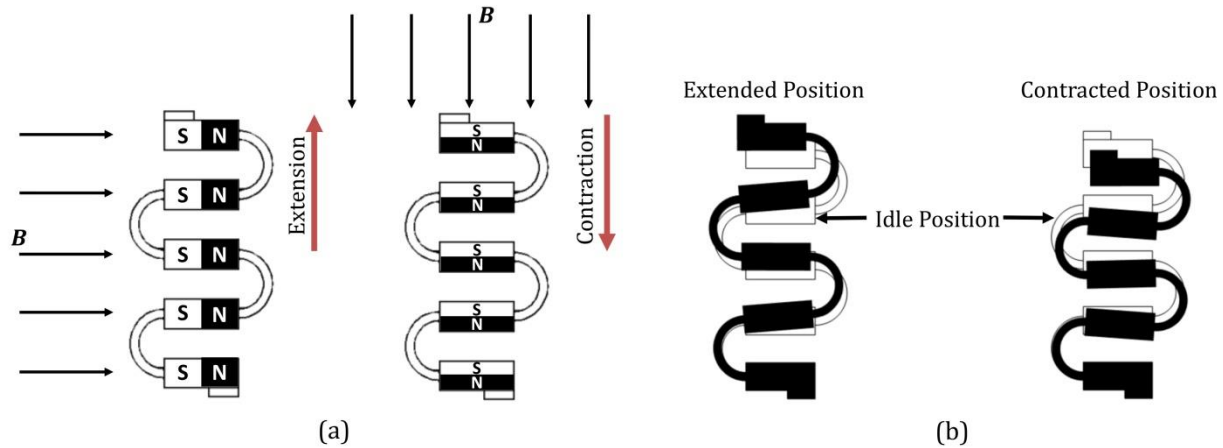


Figure 1. (a) Magnetization of the soft magnetic blocks according to the external magnetic field direction. (b) Extended, contracted and idle positions of the microactuator.

Mechanical Design

Some key advantages of the proposed microactuator design are its scalability and customizability. One can simply modify the actuator characteristics by adjusting the beam parameters (which corresponds to actuator stiffness) or parameters of the soft magnetic material. In the described design approach, we focused on the design of microactuator for a selected soft magnetic material; Nickel-Iron (Ni-Fe) 4750. As mentioned earlier, Ni-Fe alloys have excellent soft magnetic properties and low magnetostriction. A soft magnetic material block has a length of 25 μm and a width of 10 μm . All the numerical simulations were done using COMSOL Multiphysics.

Since beams have a significant effect on the characteristics of the microactuator, it is of interest to determine suitable parameters for the beams. By using the Castigliano’s theorem, the deflection of a semi-circular beam where it is fixed at one end and load acting on the other end can be determined (see Figure 2). According to the theorem, the beam deflection δ_b is given by Equation 1.

$$\delta_b = \left(\frac{\pi}{2}\right) \left(\frac{P}{EI}\right) r_b^3 \tag{Equation (1)}$$

where P is the load, E is the Young’s modulus, I is the second moment of area and r_b is the radius of the semi-circular beam. From Equation 1, it can be seen that decreasing E and I would increase the deflection for a given force. Furthermore, it also suggests that increasing r_b would result in higher beam deflections. However, since P is the magnetic force between soft magnetic blocks and increasing r_b would mean that the gap between adjacent soft magnetic blocks would increase, resulting in a reduction in P .

Beam Material Selection

For this study, three materials were selected as candidates for the beam material: Polydimethylsiloxane (PDMS), Si and SiC. A microactuator model consisting of three soft magnetic material blocks and two beams as shown in Figure 3 was considered. Through numerical simulations, the displacement of the microactuator in the y-direction was calculated for different beam widths and external magnetic field strengths for each beam material. Figure 4 represents a comparison between the materials in terms of actuator displacement. The notations y_{PDMS} , y_{Si} and y_{SiC} denote y-displacements of the PDMS, Si and SiC beam actuators respectively. The displacements achieved by the use of PDMS beams are significantly larger (in the magnitude of 10^5) than the displacements from Si and SiC beams. Among the considered

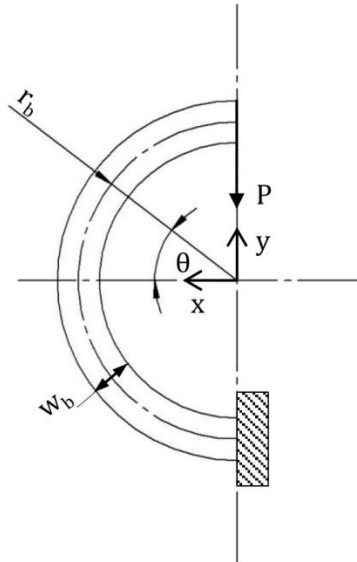


Figure 2. Schematic diagram for deflection of a curved beam.

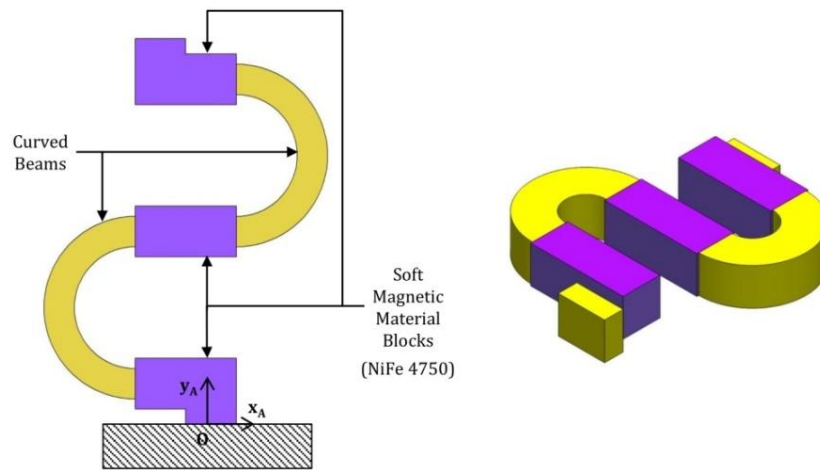


Figure 3. Model of the proposed microactuator. The soft magnetic material blocks are connected together with flexible curved beams.

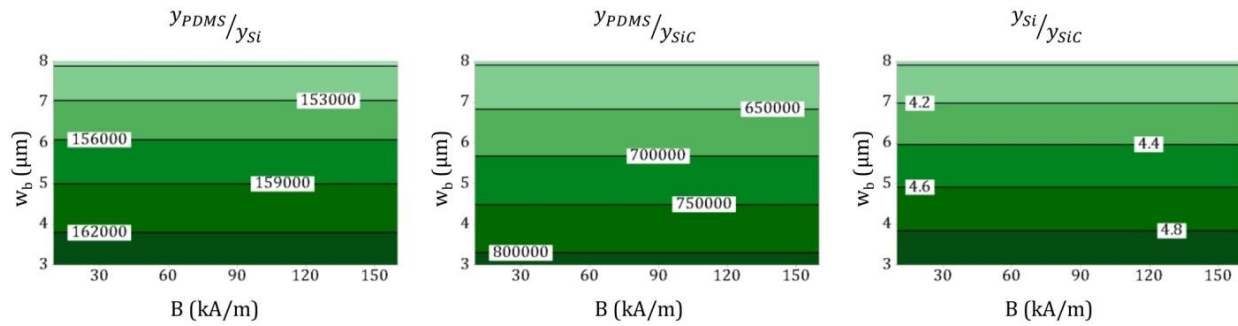


Figure 4. Performance comparison between PDMS, Si and SiC as beam material. The labels represent the displacement factor values.

three materials, SiC beams showed the least displacements. Therefore, PDMS beams are selected for the microactuator design.

Effect of Beam Width and Radius on Microactuator Characteristics

According to Equation 1, increasing the width w_b of the beam decreases the actuator displacement y_a . Meanwhile, since reducing the beam radius decreases the gap between two soft magnetic blocks, the magnetic interaction forces between the two blocks increase, thus improving the force output of the microactuator. Therefore, it is desirable to minimize both beam width and radius. Apart from that, it is of interest to investigate how increasing the number of soft magnetic blocks affects the microactuator characteristics. To this effect, two microactuator models having three and five soft magnetic material blocks (see Figure 5(a)) are used for the analysis. Here, the microactuator models having three and five soft magnetic blocks are addressed as model 1 and model 2 respectively.

First, w_b was varied from 3 μm to 10 μm while keeping the other parameters constant. The stress generated within the beams was numerically computed for each case. As it can be seen from Figure 5(b), the maximum stress within the beam has not reached the yield strength of PDMS only for $w_b = 9 \mu\text{m}$ and $w_b = 10 \mu\text{m}$ cases of model 1 and $w_b = 10 \mu\text{m}$ case of model 2. For the w_b values above that do not result in yielding of the beam. As mentioned earlier, by changing the beam radius r_b the force characteristics of the microactuator can be modified. Therefore, r_b was varied to evaluate microactuator performance based on structural integrity and force output. With the constraint of keeping the microactuator length below 100 μm , the beam radius was varied from 6 μm to 20 μm for model 1, while it was varied from 6 μm to 10 μm for model 2. According to Figure 6, for model 1, the following beam parameter combinations do not result in yielding of the beams: ($w_b = 9 \mu\text{m}$, $r_b = 10 \mu\text{m}$), ($w_b = 9 \mu\text{m}$, $r_b = 15 \mu\text{m}$), ($w_b = 9 \mu\text{m}$, $r_b = 20 \mu\text{m}$), ($w_b = 10 \mu\text{m}$, $r_b = 10 \mu\text{m}$), ($w_b = 10 \mu\text{m}$, $r_b = 15 \mu\text{m}$) and ($w_b = 10 \mu\text{m}$, $r_b = 20 \mu\text{m}$). For model 2, only ($w_b = 10 \mu\text{m}$, $r_b = 10 \mu\text{m}$) combination is possible. Then, the force outputs of the microactuators, having each of the parameter combinations selected above, were numerically computed using the contact simulation model presented in Figure 7(a). The force characteristic of model 1 is shown in Figure 7(b). It can be seen that ($w_b = 9 \mu\text{m}$, $r_b = 10 \mu\text{m}$) combination generates the highest contact force. For ($w_b = 10 \mu\text{m}$, $r_b = 10 \mu\text{m}$) combination of model 2, the force output was 553.16 nN. As expected, by observing Figure 7(b), it can be concluded that the force output increases as r_b is reduced. Furthermore, comparing model 1 and model 2 with the available force outputs, it can be said that increasing the number of soft magnetic blocks can improve the force output of the microactuator. However, the microactuator length of model 1 with ($w_b = 9 \mu\text{m}$, $r_b = 10 \mu\text{m}$) is 41.67% lower than that of model 2 with ($w_b = 10 \mu\text{m}$, $r_b = 10 \mu\text{m}$). Furthermore, force densities (defined as amount of force generated per a unit length of the microactuator) of model 1 with ($w_b = 9 \mu\text{m}$, $r_b = 10 \mu\text{m}$) and model 2 with ($w_b = 10 \mu\text{m}$, $r_b = 10 \mu\text{m}$) are 7.23 mN/m and 5.76 mN/m respectively. Therefore, considering both compactness and force characteristics, it can be determined that a microactuator having three soft magnetic material blocks, a beam width of 9 μm and beam radius of 10 μm is optimal within the considered design space. The designed microactuator has a length of 56 μm , allowing the microactuator to be used for actuating an untethered microrobot as presented in the next section.

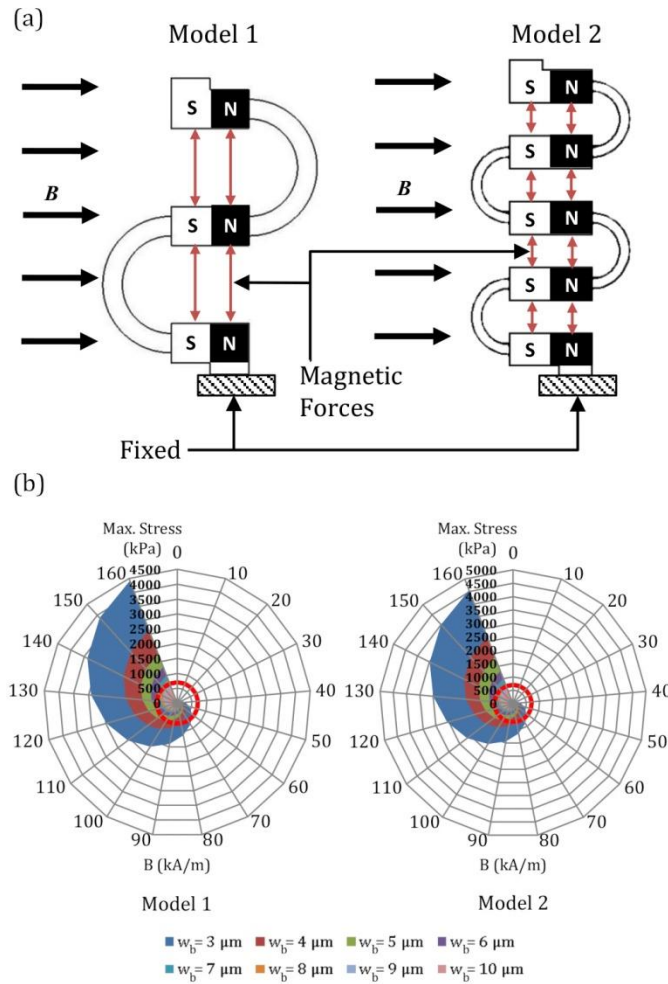


Figure 5. (a) The two actuator models considered in the study having different number of soft magnetic material blocks. The magnetization of the soft magnetic blocks under a horizontal magnetic field and repulsive magnetic interaction force generation is also shown. (b) Maximum stress distribution for different beam width values in the operating region.

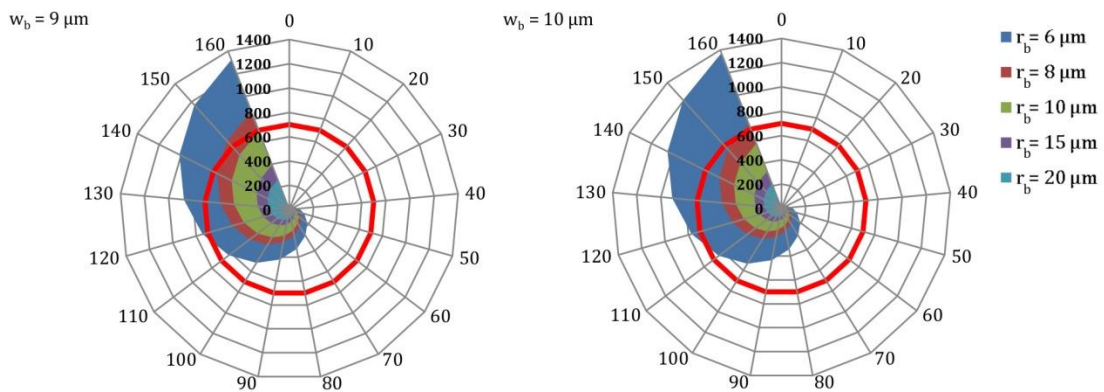


Figure 6. Maximum stress distribution in model 1 for different beam radii values in the operating region. The red color boundary represents the yield strength of PDMS which is 700 kPa.

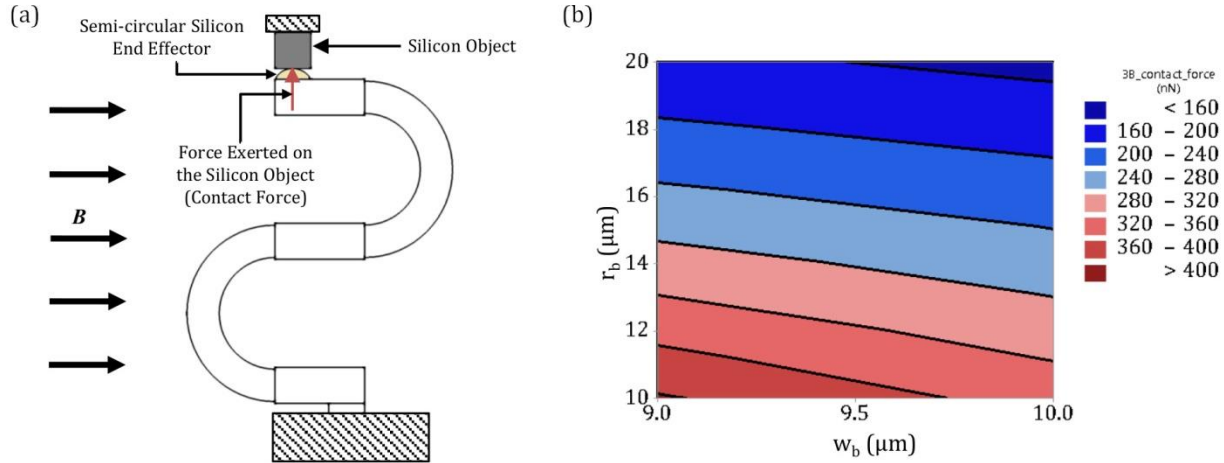


Figure 7. (a) Schematic diagram of the contact simulation model. (b) Force output variation of model 1 with beam width and radius.

Microactuator Characteristics and Performance

Actuator Displacement and Force

The characteristics of the designed microactuator were analyzed using numerical simulations under no-load condition. In terms of range of motion, the actuator displacement increases when the strength of the external magnetic field increases (see Figure 8(a)). Furthermore, it demonstrated a maximum displacement of $111.6 \mu\text{m}$ at 160 kA/m during extension mode, which is the primary operating mode. Apart from that, the microactuator is able to achieve a maximum displacement of $10.7 \mu\text{m}$ at 80 kA/m during contraction mode. Even though the relationship between actuator force F_A and B is nonlinear in the considered complete B range in the extension mode, the relationship is approximately linear in the B region $80\text{-}160 \text{ kA/m}$. This linear relationship can be expressed as given in Equation 2.

$$d_y = 1.05B - 59.87 \quad B \in [80, 160] \text{ kA/m} \quad \text{Equation (2)}$$

where d_y is the actuator displacement in the y_A -direction.

As shown in Figure 8(b), the maximum actuator force computed according to the previously mentioned contact simulation model was 404.3 nN (at 160 kA/m). Similar to the case of the actuator displacement, despite the relationship between F_A and B being nonlinear in the complete magnetic field strength region, the relationship is approximately linear in the B range $80\text{-}160 \text{ kA/m}$ using Equation 3.

$$F_A = 3.72B - 199.40 \quad B \in [80, 160] \text{ kA/m} \quad \text{Equation (3)}$$

represents this linear relationship. If the operating region is within this limit, then linear actuator displacement and force characteristics can be obtained. As a result, both position and force controlling would be relatively easier in the $B \in [80, 160] \text{ kA/m}$ region. The details of the regression analysis for the two scenarios are presented in Table 1.

Actuation of a Swimming Microrobot

The designed microactuator was integrated into a swimming microrobot as shown in Figure 9(a), in order to evaluate the performance numerically. The microrobot executes time-asymmetric rowing motion using artificial appendages to propel in a non-Newtonian fluid. One end of the microactuator was connected to the artificial appendage and the other end was connected to the microrobot's body, with an angle of 30°

from the horizontal. A resistive force of 250 nN/m was applied as a uniformly distributed load, which corresponds to the resistive forces generated due to a swimming motion. The computation method of the

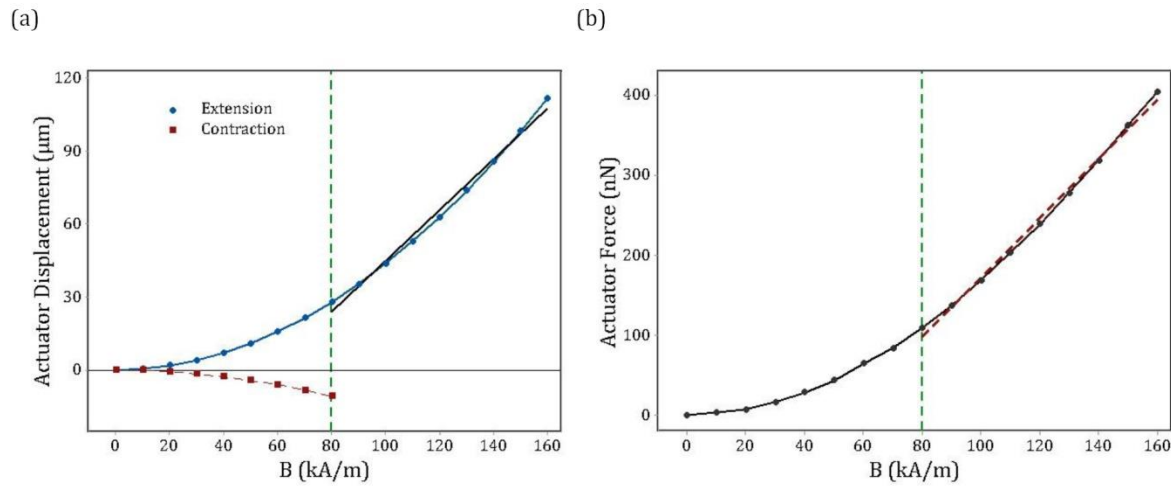


Figure 8. (a) Actuator displacement variation with external magnetic field strength. The black line indicates the linear regression fit. (b) Actuator force output variation with external magnetic field strength. The red dash line indicates the linear regression fit.

Table 1. Analysis of Variance for Actuator Displacement and Force Regression

d_y and B						F_A and B					
ANOVA						ANOVA					
Source	df	SS	MS	F	p	Source	df	SS	MS	F	p
Regression	1	6565.75	6565.75	783.46	0.000	Regression	1	82942.2	82942.2	1554.9	0.000
Error	7	58.66	8.38			Error	7	373.5	53.4		
Total	8	6624.41				Total	8	83315.6			
Pearson correlation			0.996			Pearson correlation			0.998		
R ²			0.991			R ²			0.996		

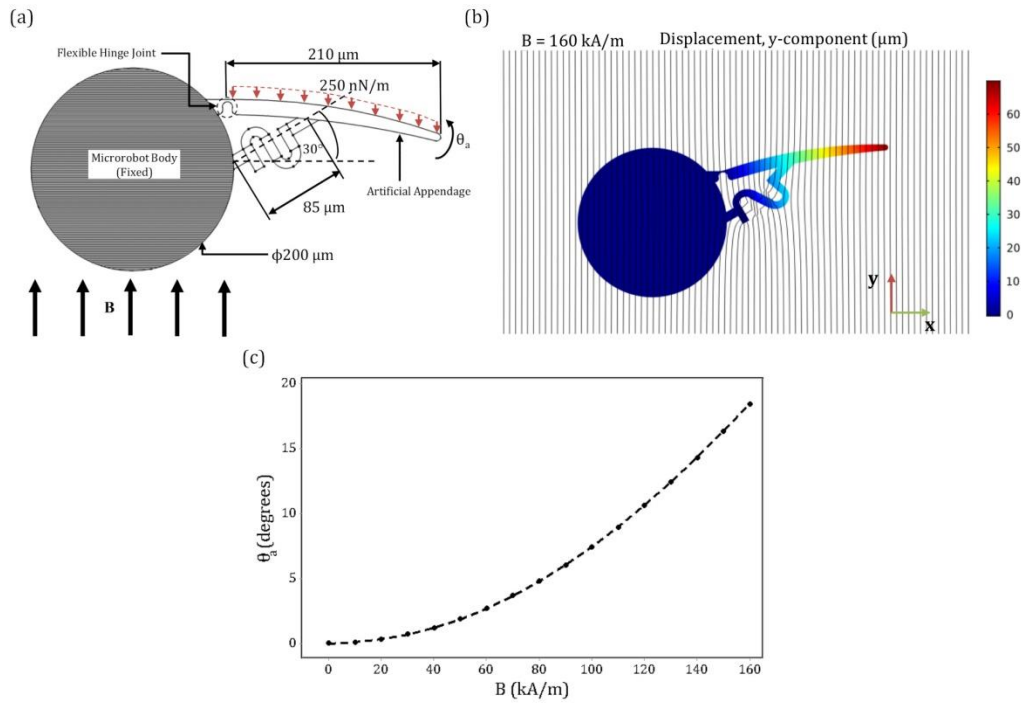


Figure 9. (a) Schematic diagram of the microactuator integrated with a swimming microrobot. The artificial appendage should undergo rowing motion. (b) Displacement profile of the artificial appendage in y -direction. The black lines represent the magnetic flux. (c) Relationship between θ_A and B .

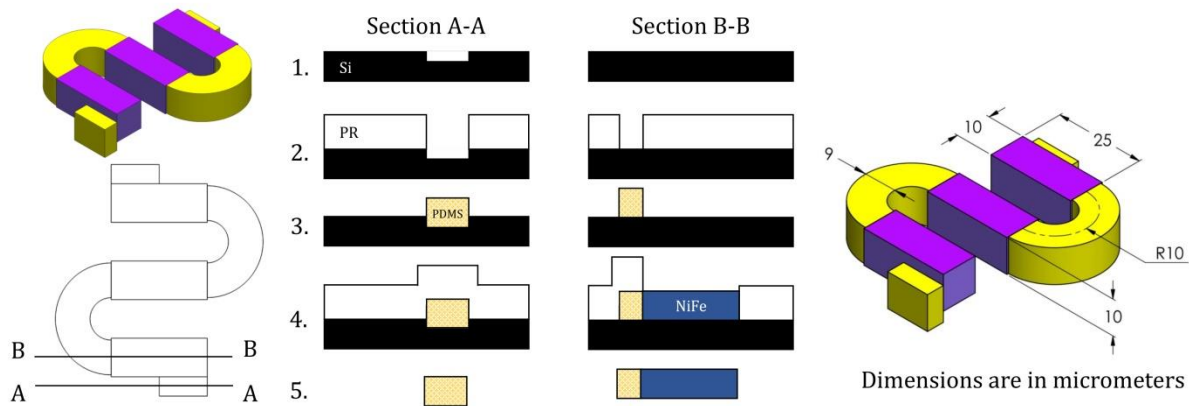


Figure 10. Dimensions and fabrication methodology of the proposed magnetic microactuator.

force magnitude (of 250 nN/m) and details of the swimming microrobot with artificial appendage are presented in our previous work [27]. The material of the artificial appendage was low-density polyethylene (LDPE). When an external magnetic field along the longitudinal direction of microrobot as shown in Figure 9(a), the artificial appendage is actuated by a stroke angle of θ_A . Figure 9(b) shows the displacement (y -component) profile of the artificial appendage at the magnetic field strength of 160 kA/m . The relationship between θ_A and B is nonlinear (see Figure 9(c)). Using the microactuator, a maximum stroke angle of 18.4°

is achievable for the considered configuration, highlighting its capability of untethered actuation of a swimming microrobot.

Apart from the highlighted integration into a swimming microrobot, the designed actuator can be used to actuate other types of micron scale devices (that require linear actuation) such as microgrippers [28-30].

Fabrication Method

The microactuator is almost a 2.5D structure with constant thickness. However, either end has out-of-plane extensions to elevate the rest of the structure, thus reducing stiction and friction effects when the actuator is in motion. Taking these conditions and the materials into consideration, a simple microfabrication method is proposed as shown in Figure 10. The sectional views illustrate the microfabrication steps in detail. In step 1, holes are created to facilitate the out-of-plane extrusions. After etching out the holes in the Silicon wafer using isotropic wet/dry etching, a positive photoresist (PR) layer is applied. Then, a 10 μm PDMS layer is coated on the substrate by spin coating method [31] after exposing the semi-circular beams and the end attachments areas as shown in step 2. After cleaning the photoresist, all the required PDMS layers are on the substrate (step 3). Then a positive photoresist is applied, defining only the locations of the soft magnetic material blocks. After that, in step 4, Ni-Fe is electrodeposited [32] to a thickness of 10 μm . Finally, the microactuator can be removed from the Si wafer in step 5. A sacrificial layer can be introduced underneath the microactuator element for easy removal if it is integrated into another structure such as a microrobot body.

Conclusion

The proposed magnetically actuated microactuator primarily consists of three soft magnetic material (Ni-Fe 4750) blocks which are connected together by two Polydimethylsiloxane (PDMS) semi-circular beams. In the presence of an external magnetic field, Ni-Fe blocks get magnetized and the generated magnetic interaction forces actuate the end effector of the microactuator. The microactuator was designed to operate in low-intensity magnetic fields up to 160 kA/m (or approximately 200 mT). A comparison between two microactuator models consisting of three and five Ni-Fe blocks showed that the model with three Ni-Fe blocks is better in terms of compactness and force characteristics. The optimal beam width and radius values were 9 μm and 10 μm respectively. Under no-load condition, the microactuator demonstrated a maximum displacement of 111.6 μm at 160 kA/m during extension mode and 10.7 μm at 80 kA/m during contraction mode. The relationship between actuator force and magnetic field strength is nonlinear, but it is approximately linear in the 80-160 kA/m region. This is also valid for the actuator displacement characteristic as well. Furthermore, the maximum force that can be exerted by the microactuator is 404.3 nN at 160 kA/m. An analysis done by integrating the microactuator with a swimming microrobot showed that it could achieve stroke angles up to 18.4° in the considered configuration, demonstrating the capability of the microactuator to be used in microrobotic applications.

Conflicts of Interest

K. N. M. Perera, H. A. G. C. Premachandra and Y. W. R. Amarasinghe filed a patent application based on the magnetic microactuator design.

Acknowledgement

The authors would like to express their gratitude to the Accelerating Higher Education Expansion and Development

(AHEAD) - Development Oriented Research (DOR) grant of the Centre for Advanced Mechatronic Systems (CFAMS), University of Moratuwa, Sri Lanka for their financial contribution and the CFAMS for their valuable advice and guidance towards the success of the research.

References

- [1] H. Ceylan, J. Giltinan, K. Kozielski, and M. Sitti, "Mobile microrobots for bioengineering applications," *Lab Chip*, **2017**, 17 (10), 1705-1724.
- [2] S. D. d. Rivaz, B. Goldberg, N. Doshi, K. Jayaram, J. Zhou, and R. J. Wood, "Inverted and vertical climbing of a quadrupedal microrobot using electroadhesion," *Science Robotics*, **2018**, 3 (25).
- [3] J. Qu, J. Choi, and K. R. Oldham, "Dynamic Structural and Contact Modeling for a Silicon Hexapod Microrobot," *Journal of Mechanisms and Robotics*, **2017**, 9 (6).
- [4] J. Jeong, D. Jang, D. Kim, D. Lee, and S. K. Chung, "Acoustic bubble-based drug manipulation: Carrying, releasing and penetrating for targeted drug delivery using an electromagnetically actuated microrobot," *Sensors and Actuators A: Physical*, **2020**, 306.
- [5] T. Qiu, S. Palagi, J. Sachs, and P. Fischer, "Soft Miniaturized Linear Actuators Wirelessly Powered by Rotating Permanent Magnets," in 2018 IEEE International Conference on Robotics and Automation (ICRA), Brisbane, Australia, **2018**.
- [6] J. Li, W. Liu, T. Li, I. Rozen, J. Zhao, B. Bahari, B. Kante, and J. Wang, "Swimming Microrobot Optical Nanoscopy," *Nano Lett*, **2016**, 16 (10), 6604-6609.
- [7] K. N. M. Perera, H. A. G. C. Premachandra, and Y. W. R. Amarasinghe, "Design of a Magnetostrictive Bimorph for Micromanipulation," in 14th KDU IRC, Ratmalana, Sri Lanka, **2021**.
- [8] Z. Nagy, D. R. Frutiger, R. I. Leine, C. Glocker, and B. J. Nelson, "Modeling and analysis of wireless resonant magnetic microactuators," in 2010 IEEE International Conference on Robotics and Automation, Anchorage, USA, **2010**.
- [9] B. R. Donald, C. G. Levey, C. D. McGray, I. Paprotny, and D. Rus, "An Untethered, Electrostatic, Globally Controllable MEMS Micro-Robot," *Journal of Microelectromechanical Systems*, **2006**, 15 (1), 1-15.
- [10] A. Aghakhani, O. Yasa, P. Wrede, and M. Sitti, "Acoustically powered surface-slipping mobile microrobots," *Proceedings of the National Academy of Sciences*, **2020**, 117 (7), 3469-3477.
- [11] R. Zhang, A. Sherehiy, Z. Yang, D. Wei, C. K. Harnett, and D. O. Popa, "ChevBot – An Untethered Microrobot Powered by Laser for Microfactory Applications," in 2019 International Conference on Robotics and Automation (ICRA), Montreal, Canada, **2019**.
- [12] G. Go, V. D. Nguyen, Z. Jin, J.-O. Park, and S. Park, "A Thermo-electromagnetically Actuated Microrobot for the Targeted Transport of Therapeutic Agents," *International Journal of Control, Automation and Systems*, **2018**, 16 (3), 1341-1354.
- [13] K. E. Peyer, L. Zhang, and B. J. Nelson, "Bio-inspired magnetic swimming microrobots for biomedical applications," *Nanoscale*, **2013**, 5 (4), 1259-72.
- [14] L. Chang, and Y. W. Yi, "Micromachined magnetic actuators using electroplated Permalloy," *IEEE Transactions on Magnetics*, **1999**, 35 (3), 1976-1985.
- [15] M. Megregany, P. Nagarkar, S. D. Senturia, and J. H. Lang, "Operation of microfabricated harmonic and ordinary side-drive motors," in IEEE Proceedings on Micro Electro Mechanical Systems, An Investigation of Micro Structures, Sensors, Actuators, Machines and Robots, Napa Valley, USA, **1990**.
- [16] H. Guckel, K. J. Skrobis, T. R. Christenson, J. L. Klein, S. Han, B. Choi, E. G. Lovell, and T. W. Chapman, "Fabrication and testing of the planar magnetic micromotor," *Journal of Micromechanics and Microengineering*, **1991**, 1, 135-138.
- [17] J. W. Judy, and R. S. Muller, "Magnetically actuated, addressable microstructures," *Journal of Microelectromechanical Systems*, **1997**, 6 (3), 249-256.
- [18] F. Liu, G. Alici, B. Zhang, S. Beirne and W. Li, "Corrigendum: Fabrication and characterization of a magnetic micro-actuator based on deformable Fe-doped PDMS artificial cilium using 3D printing," *Smart Materials and Structures*, **2015**, 24 (6).
- [19] H. Ceylan, N. O. Dogan, I. C. Yasa, M. N. Musaoglu, Z. U. Kulali and M. Sitti, "3D printed personalized magnetic micromachines from patient blood-derived biomaterials," *Science Advances*, **2021**, 7 (36).
- [20] H. Feng, X. Miao and Z. Yang, "Design, Simulation and Experimental Study of the Linear Magnetic Microactuator," *Micromachines*, **2018**, 9 (9), 454-463.

- [21] O. Cugat, J. Delamare, and G. Reyne, "Magnetic micro-actuators and systems (MAGMAS)," *IEEE Transactions on Magnetics*, **2003**, 39 (6), 3607-3612.
- [22] D. Niarchos, "Magnetic MEMS: key issues and some applications," *Sensors and Actuators A: Physical*, **2003**, 106 (1-3), 255-262.
- [23] K. Samsami, S. A. Mirbagheri, F. Meshkati, and H. C. Fu, "Stability of Soft Magnetic Helical Microrobots," *Fluids*, **2020**, 5 (1).
- [24] H. W. Tung, M. Maffioli, D. R. Frutiger, K. M. Sivaraman, S. Pane, and B. J. Nelson, "Polymer-Based Wireless Resonant Magnetic Microrobots," *IEEE Transactions on Robotics*, **2014**, 30 (1), 26-32.
- [25] L. Mellal, D. Folio, K. Belharet, and A. Ferreira, "Modeling and Characterization of Deformable Soft Magnetic Microrobot for Targeted Therapy," *IEEE Robotics and Automation Letters*, **2021**, 6 (4), 8293-8300.
- [26] M. Sarracanie and N. Salameh, "Low-Field MRI: How Low Can We Go? A Fresh View on an Old Debate," *Frontiers in Physics*, **2020**, 8.
- [27] K. N. M. Perera, Y. W. R. Amarasinghe and D. V. Dao, "An Artificial Appendage for Swimming Microrobots in Non-Newtonian Fluids," in 2021 Moratuwa Engineering Research Conference (MERCon), Moratuwa, Sri Lanka, **2021**.
- [28] G. Shao, H. O. T. Ware, J. Huang, R. Hai, L. Li and C. Sun, "3D printed magnetically-actuating micro-gripper operates in air and water," *Additive Manufacturing*, **2021**, 38.
- [29] C. Elbuken, L. Gui, C. Ren, M. Yavuz and M. Khamesee, "Design and analysis of a polymeric photo-thermal microactuator," *Sensors and Actuators A: Physical*, **2008**, 147 (1), 292-299.
- [30] A. Ichikawa, S. Sakuma, M. Sugita, T. Shoda, T. Tamakoshi, S. Akagi and F. Arai, "On-chip enucleation of an oocyte by untethered microrobots," *Journal of Micromechanics and Microengineering*, **2014**, 24 (9).
- [31] H. Takao, K. Miyamura, H. Ebi, M. Ashiki, K. Sawada and M. Ishida, "A MEMS microvalve with PDMS diaphragm and two-chamber configuration of thermo-pneumatic actuator for integrated blood test system on silicon," *Sensors and Actuators A: Physical*, **2005**, 119 (2), 468-475.
- [32] G. Schiavone, J. Murray, R. Perry, A. R. Mount, M. P. Y. Desmulliez and A. J. Walton, "Integration of Electrodeposited Ni-Fe in MEMS with Low-Temperature Deposition and Etch Processes," *Materials*, **2017**, 10 (3), 323-341.